

# Single Higgs boson production in association with a top quark through FCNSI

V. M. López-Guerrero\*

*Facultad de Ciencias Físico-Matemáticas, Benemérita Universidad  
Autónoma de Puebla, C.P. 72570, Puebla, México, and  
Centro Internacional de Física Fundamental (CIFFU),  
Benemérita Universidad Autónoma de Puebla, C.P. 72570, Puebla, México.*

M. A. Arroyo-Ureña†

*Facultad de Ciencias Físico-Matemáticas, Benemérita Universidad  
Autónoma de Puebla, C.P. 72570, Puebla, México, and  
Centro Interdisciplinario de Investigación y Enseñanza de la Ciencia (CIIEC),  
Benemérita Universidad Autónoma de Puebla, C.P. 72570, Puebla, México.*

J. L. Díaz-Cruz‡

*Facultad de Ciencias Físico-Matemáticas, Benemérita Universidad  
Autónoma de Puebla, C.P. 72570, Puebla, México, and  
Centro Interdisciplinario de Investigación y Enseñanza de la Ciencia (CIIEC),  
Benemérita Universidad Autónoma de Puebla, C.P. 72570, Puebla, México.*

O. Félix-Beltrán§

*Facultad de Ciencias de la Electrónica and  
Centro Internacional de Física Fundamental (CIFFU),  
Benemérita Universidad Autónoma de Puebla, C.P. 72570, Puebla, México.*

T. A. Valencia-Pérez¶

*Instituto de Física, Universidad Nacional Autónoma de México, C.P. 01000, CDMX, México.*

## Abstract

We study the production and possible detection of a single Higgs boson in association with a top quark in proton-proton collisions ( $pp \rightarrow th + X$ ) at the High-Luminosity Large Hadron Collider. This process absent in the Standard Model is predicted by other models such as the Two-Higgs Doublet Model of type III, which is the theoretical framework adopted in this work. Promising results are found for specific scenarios of the model parameter space, which consist mainly of the parameters  $\tan\beta$ ,  $\cos(\alpha - \beta)$  and the parameter  $\chi_{tc}$ , responsible for the Flavor-Changing Neutral Scalar Interactions (FCNSI). Using the machine learning *Boosted Decision Trees* algorithm, we predict *signal significances* at level of  $5\sigma$  for  $\tan\beta = 1$ ,  $\cos(\alpha - \beta) = 0.1$  and  $\chi_{tc} = 5$  and integrated luminosities in the range  $2500 \text{ fb}^{-1} \leq \mathcal{L}_{\text{int}} \leq 3000 \text{ fb}^{-1}$ .

Keywords: LHC, HL-LHC, 2HDM-III, FCNC

---

\* victor.lopezguer@alumno.buap.mx

† marco.arroyo@fcfm.buap.mx

‡ jldiaz@fcfm.buap.mx

§ olga.felix@correo.buap.mx

¶ tvalencia@fisica.unam.mx

## I. INTRODUCTION

More than twelve years ago, the ATLAS and CMS collaborations announced the observation of a new spin-0 particle with mass  $m = 125.10 \pm 0.14 \text{ GeV}$  consistent with the Higgs boson properties predicted by the Standard Model (SM) [1, 2]. After the discovery of the Higgs boson an objective of the Large Hadron Collider (LHC) is to characterize its properties because, among other things, the Higgs field is fundamental to the generation of the particle masses contained in the SM [3–6]. As we know the SM provides a detailed description of the weak, strong and electromagnetic interactions, also successfully explains many of the experimental observations made in particle physics. However, despite these achievements, there are phenomena that cannot be explained within the SM, which is commonly referred as Beyond Standard Model (BSM) physics [7–12]. The fact that the SM leaves open questions for some phenomena directs our attention to exploring additional models, particularly those with an extended Higgs sector. One of them is the Two-Higgs Doublet Model of type III (2HDM-III) [13–17], which predicts Flavor-Changing Neutral Currents (FCNC) at tree-level. The 2HDM-III leads to study interactions not found in the SM and to perform analysis of processes that could enhance the SM-like Higgs boson signals. It is also attractive to investigate Flavor-Violating (FV) processes involving top quarks because these kinds of interactions have large rates predicted by the model and at the same time allowed by experimental constraints. In contrast, FV processes are strongly suppressed in the SM due to the Glashow-Iliopoulos-Maiani (GIM) mechanism [18] and FCNSI are forbidden. Recently, the ATLAS [19] and CMS [20] collaborations reported upper limits on the  $\mathcal{BR}(t \rightarrow ch)$ , particularly CMS reported a  $\mathcal{BR}(t \rightarrow ch) < 0.00046$  at 95% of confidence level, whose importance for this work lies in the fact that this result imposes limits on the parameter  $\chi_{tc}$ , responsible for the Flavor-Changing interaction in the process to study. A review of the process  $pp \rightarrow th + X$  is presented in Ref. [21] while the authors of Ref. [22] studied the process from an effective field theory viewpoint, analyzing the impact of the coupling  $\lambda_{tqh}$  on the production cross-section and the *signal significance*. However, as shown later, sophisticated machine learning techniques allow one to explore smaller values for the  $\lambda_{tqh}$  coupling.

In this paper, we are interested in the single Higgs boson production in association with a top quark via proton-proton collisions at the High Luminosity LHC (HL-LHC) [23]. Specific channels of decay are considered, that is,  $pp \rightarrow th + X$  ( $t \rightarrow \ell\nu_\ell b$ ,  $h \rightarrow \gamma\gamma$ ). Although the branching ratio of the Higgs boson into photons is relatively small  $\mathcal{O}(10^{-3})$ , it has the advantages of good resolution on the Higgs mass and small QCD backgrounds. In fact, this channel is essential for signal isolation, as will be seen later.

This work is structured as follows. In Sec. II, we conduct a comprehensive review of the 2HDM-III with a particular emphasis on the theoretical implications of employing a four-zero texture in the Yukawa Lagrangian. Experimental constraints on the model parameter space are also included. Section III focuses on taking advantage of the insights gained from previous sections, performing a computational analysis of the proposed signal and its SM background processes. Finally, the conclusions are presented in Sec. IV.

## II. THE MODEL

The 2HDM introduces an additional Higgs doublet with the same hypercharge +1:  $\Phi_a^T = (\phi_a^+, \phi_a^0)$  ( $a = 1, 2$ ), where  $\phi_a^0$  denotes the neutral part and  $\phi_a^\pm$  denotes the charged part. Depending of the vacuum expectation values (VEVs) chosen for the two Higgs doublets we can have two basis: (*i*) in the Higgs basis

only one of the two Higgs doublets acquires a VEV, (*ii*) whereas in the generic basis both of the Higgs doublets acquire a VEV. The 2HDM built on the generic basis is called “the general 2HDM” [24]. In this section, we present the scalar potential and the Yukawa Lagrangian for the 2HDM type III.

### A. Scalar potential

The most general  $SU(2)_L \times U(1)_Y$  invariant scalar potential of the 2HDM is given by [24, 25]

$$\begin{aligned}
V = & \mu_1^2(\Phi_1^\dagger\Phi_1) + \mu_2^2(\Phi_2^\dagger\Phi_2) - (\mu_{12}^2(\Phi_1^\dagger\Phi_2 + \text{H.c.})) \\
& + \frac{1}{2}\lambda_1(\Phi_1^\dagger\Phi_1)^2 + \frac{1}{2}\lambda_2(\Phi_2^\dagger\Phi_2)^2 + \lambda_3(\Phi_1^\dagger\Phi_1)(\Phi_2^\dagger\Phi_2) + \lambda_4(\Phi_1^\dagger\Phi_2)(\Phi_2^\dagger\Phi_1) \\
& + \left( \frac{1}{2}\lambda_5(\Phi_1^\dagger\Phi_2)^2 + \lambda_6(\Phi_1^\dagger\Phi_1)(\Phi_1^\dagger\Phi_2) + \lambda_7(\Phi_2^\dagger\Phi_2)(\Phi_1^\dagger\Phi_2) + \text{H.c.} \right).
\end{aligned} \tag{1}$$

Hermiticity condition for the potential implies that the  $\lambda_{1,2,3,4}$ ,  $\mu_{1,2}$  parameters are real, while the  $\lambda_{5,6,7}$  and  $\mu_{12}^2$  parameters can be complex numbers. We choose to work in a general 2HDM CP-conserving with a softly broken  $Z_2$  symmetry.

After the Electroweak Symmetry Breaking (EWSB), the two Higgs doublets acquire VEVs given as

$$\langle \Phi_a \rangle = \frac{1}{\sqrt{2}} \begin{pmatrix} 0 \\ v_a \end{pmatrix}, \quad a = 1, 2, \tag{2}$$

where  $v_{1,2}$  are real and satisfy  $v = \sqrt{v_1^2 + v_2^2} = 246$  GeV [26]. The VEV ratio defines the parameter  $\tan \beta \equiv v_2/v_1$ .

The mass matrix in the CP-even sector is given by

$$\mathcal{M}_{even} = \begin{pmatrix} m_{11} & m_{12} \\ m_{12} & m_{22} \end{pmatrix}, \tag{3}$$

where

$$\begin{aligned}
m_{11} &= 2\lambda_1 v^2 \cos^2 \beta + 2\mu_{12}^2 \frac{\sin \beta}{\cos \beta}, \\
m_{12} &= 2(\lambda_3 + \lambda_4 + \lambda_5) v^2 \cos \beta \sin \beta - \mu_{12}^2, \\
m_{22} &= 2\lambda_2 v^2 \sin^2 \beta + 2\mu_{12}^2 \frac{\cos \beta}{\sin \beta}.
\end{aligned} \tag{4}$$

After diagonalization of the mass matrix  $\mathcal{M}_{even}$  and defining a mixing angle  $\alpha$ , we translate the gauge states into the mass eigenstates  $h^0$  and  $H^0$ :

$$\begin{pmatrix} H^0 \\ h^0 \end{pmatrix} = \begin{pmatrix} \cos \alpha & \sin \alpha \\ -\sin \alpha & \cos \alpha \end{pmatrix} \begin{pmatrix} \text{Re}(\phi_1^0) \\ \text{Re}(\phi_2^0) \end{pmatrix}, \tag{5}$$

with

$$\tan 2\alpha = \frac{2m_{12}}{m_{11} - m_{22}}. \tag{6}$$

Likewise, the mixing angle  $\beta$  rotates the charged components of  $\Phi_a$  into the charged mass eigenstates  $G_W^\pm$  and  $H^\pm$  as follows:

$$\begin{pmatrix} G_W^\pm \\ H^\pm \end{pmatrix} = \begin{pmatrix} \cos \beta & \sin \beta \\ -\sin \beta & \cos \beta \end{pmatrix} \begin{pmatrix} \phi_1^\pm \\ \phi_2^\pm \end{pmatrix}. \quad (7)$$

On the other hand, to obtain the neutral mass eigenstates  $G_Z$  and  $A$  we make the following rotation:

$$\begin{pmatrix} G_{Z^0} \\ A^0 \end{pmatrix} = \begin{pmatrix} \cos \beta & \sin \beta \\ -\sin \beta & \cos \beta \end{pmatrix} \begin{pmatrix} \text{Im}(\phi_1^0) \\ \text{Im}(\phi_2^0) \end{pmatrix}. \quad (8)$$

We obtain the physical masses  $M_{H^\pm}$ ,  $M_{h^0}$ ,  $M_{H^0}$  and  $M_{A^0}$ , given by the equations:

$$M_{H^0, h^0}^2 = \frac{1}{2} \left( m_{11} + m_{22} \pm \sqrt{(m_{11} - m_{22})^2 + 4m_{12}^2} \right), \quad (9)$$

$$M_{H^\pm}^2 = \frac{\mu_{12}^2}{\sin \beta \cos \beta} - \frac{1}{2} v^2 (\lambda_4 + \lambda_5), \quad (10)$$

$$M_{A^0}^2 = M_{H^\pm}^2 + \frac{1}{2} v^2 (\lambda_4 - \lambda_5). \quad (11)$$

Four new particles emerge from the introduction of a second Higgs doublet,  $H^0$ ,  $A^0$  and  $H^\pm$ . Detection of these new particles is a goal of future experiments such as HL-LHC [27] and FCC [28, 29].

## B. Yukawa Lagrangian

The different versions of the 2HDM can be defined through the Higgs doublets and fermionic field interactions, as shown in Table I.

Model	$u_R^i$	$d_R^i$	$l_R^i$
Flavor conserving models			
I	$\Phi_2$	$\Phi_2$	$\Phi_2$
II	$\Phi_2$	$\Phi_1$	$\Phi_1$
Lepton-specific	$\Phi_2$	$\Phi_2$	$\Phi_1$
Flipped	$\Phi_2$	$\Phi_1$	$\Phi_2$
Flavor violating model			
III	$\Phi_1, \Phi_2$	$\Phi_1, \Phi_2$	$\Phi_1, \Phi_2$

TABLE I. 2HDM definitions based on the Higgs doublets couplings with fermions in the Yukawa sector.

For the 2HDM-III, the Yukawa Lagrangian is written as [30]:

$$\begin{aligned} \mathcal{L}_Y = & - \left( Y_1^u \bar{Q}_L \tilde{\Phi}_1 u_R + Y_2^u \bar{Q}_L \tilde{\Phi}_2 u_R + Y_1^d \bar{Q}_L \Phi_1 d_R + Y_2^d \bar{Q}_L \Phi_2 d_R \right. \\ & \left. + Y_1^l \bar{L}_L \Phi_1 l_R + Y_2^l \bar{L}_L \Phi_2 l_R + \text{H.c.} \right), \end{aligned} \quad (12)$$

where  $\tilde{\Phi}_a = i\sigma_2 \Phi_a^*$ ,  $Q_L$  is the weak isospin quark doublet,  $L_L$  is the weak isospin lepton doublet,  $u_R$ ,  $d_R$  are weak isospin quark singlets,  $l_R$  is the weak isospin lepton singlet and  $Y_a^f$  ( $f = u, d, \ell$ ) are the  $3 \times 3$  Yukawa matrices.

From the Yukawa Lagrangian in Eq. (12) and after the EWSB, the fermion mass matrices come into:

$$M_f = \frac{1}{\sqrt{2}} \left( v_1 Y_1^f + v_2 Y_2^f \right), \quad f = u, d, \ell. \quad (13)$$

We assume that both Yukawa matrices have a four-zero texture [31] and that they are Hermitian. The sum of such matrices inherits its structure to the mass matrix as follows

$$M_f = \begin{pmatrix} 0 & D_f & 0 \\ D_f & C_f & B_f \\ 0 & B_f & A_f \end{pmatrix}, \quad (14)$$

The elements of the matrix in Eq. (14) are related to the fermion masses  $m_{f_i}$  ( $i = 1, 2, 3$ ), through the principal invariants:

$$\begin{aligned} \text{Tr}(M_f) &= C_f + A_f = m_{f_1} + m_{f_2} + m_{f_3}, \\ \lambda(M_f) &= C_f A_f - D_f^2 - B_f = m_{f_1} m_{f_2} + m_{f_1} m_{f_3} + m_{f_2} m_{f_3}, \\ \det(M_f) &= -D_f^2 A_f = m_{f_1} m_{f_2} m_{f_3}. \end{aligned} \quad (15)$$

From Eq. (15) we find a relation between the components of the mass matrix of four-zero textures and the fermion masses as follows:

$$\begin{aligned} A_f &= m_{f_3} - m_{f_2}, \\ B_f &= m_{f_3} \sqrt{\frac{r_2(r_2 + r_1 - 1)(r_2 + r_2 - 1)}{1 - r_2}}, \\ C_f &= m_{f_3}(r_2 + r_1 + r_2), \\ D_f &= \sqrt{\frac{m_{f_1} m_{f_2}}{1 - r_2}}, \end{aligned} \quad (16)$$

where  $r_i = m_{f_i}/m_{f_3}$ .

Performing a bi-unitary transformation we diagonalize the fermion mass matrices as

$$\bar{M}_f = V_{fL}^\dagger M_f V_{fR} = \frac{1}{\sqrt{2}} \left( v_1 \tilde{Y}_1^f + v_2 \tilde{Y}_2^f \right), \quad (17)$$

where  $\bar{M}_f = \text{diag}(m_{f_1}, m_{f_2}, m_{f_3})$  and  $\tilde{Y}_a^f = V_{fL}^\dagger Y_a^f V_{fR}$ . However, the Yukawa matrices are not necessarily diagonalized. As a consequence, FCNSI will be induced at tree-level. The fact that  $M_f$  is assumed as Hermitian, implies that  $V_{fL} = V_{fR} \equiv V_f$ . Here,  $V_f = \mathcal{O}_f P_f$ , where  $P_f = \text{diag}\{e^{i\alpha_f}, e^{i\beta_f}, 1\}$  and

$$\mathcal{O}_f = \begin{pmatrix} \sqrt{\frac{m_{f_2} m_{f_3} (A - m_{f_1})}{A(m_{f_2} - m_{f_1})(m_{f_3} - m_{f_1})}} & \sqrt{\frac{m_{f_1} m_{f_3} (m_{f_2} - A)}{A(m_{f_2} - m_{f_1})(m_{f_3} - m_{f_2})}} & \sqrt{\frac{m_{f_1} m_{f_3} (A - m_{f_3})}{A(m_{f_3} - m_{f_1})(m_{f_3} - m_{f_2})}} \\ -\sqrt{\frac{m_{f_1} (m_{f_1} - A)}{(m_{f_2} - m_{f_1})(m_{f_3} - m_{f_1})}} & \sqrt{\frac{m_{f_2} (A - m_{f_2})}{(m_{f_2} - m_{f_1})(m_{f_3} - m_{f_2})}} & \sqrt{\frac{m_{f_3} (m_{f_2} - A)}{(m_{f_2} - m_{f_1})(m_{f_3} - m_{f_2})}} \\ \sqrt{\frac{m_{f_1} (A - m_{f_2})(A - m_{f_3})}{A(m_{f_2} - m_{f_1})(m_{f_3} - m_{f_1})}} & -\sqrt{\frac{m_{f_2} (A - m_{f_1})(m_{f_3} - A)}{A(m_{f_2} - m_{f_1})(m_{f_3} - m_{f_2})}} & \sqrt{\frac{m_{f_3} (A - m_{f_1})(A - m_{f_2})}{A(m_{f_3} - m_{f_1})(m_{f_3} - m_{f_2})}} \end{pmatrix}. \quad (18)$$

An important point is that  $V_{u,d}$  must reproduce the observed CKM matrix elements ( $V_{\text{CKM}}$ ), which is obtained as  $V_{\text{CKM}} = V_u^\dagger V_d$ , as shown in Ref. [17].

From Eq. (17), we obtain the following expression

$$[\tilde{Y}_a^f]_{ij} = \frac{\sqrt{2}}{v_a} \delta_{ij} \bar{M}_{ij}^f - \frac{v_b}{v_a} [\tilde{Y}_b^f]_{ij}, \quad i, j = 1, 2, 3, \quad b = 1, 2, \quad (19)$$

2HDM-III	$X$	$Y$	$Z$	$\xi_h^u$	$\xi_h^d$	$\xi_h^l$	$\xi_H^u$	$\xi_H^d$	$\xi_H^l$
2HDM-I-like	$-\cot\beta$	$\cot\beta$	$-\cot\beta$	$c_\alpha/s_\beta$	$c_\alpha/s_\beta$	$c_\alpha/s_\beta$	$s_\alpha/s_\beta$	$s_\alpha/s_\beta$	$s_\alpha/s_\beta$
2HDM-II-like	$\tan\beta$	$\cot\beta$	$\tan\beta$	$c_\alpha/s_\beta$	$-s_\alpha/c_\beta$	$-s_\alpha/c_\beta$	$s_\alpha/s_\beta$	$c_\alpha/c_\beta$	$c_\alpha/c_\beta$
2HDM-X-like	$-\cot\beta$	$\cot\beta$	$\tan\beta$	$c_\alpha/s_\beta$	$c_\alpha/s_\beta$	$-s_\alpha/c_\beta$	$s_\alpha/s_\beta$	$s_\alpha/s_\beta$	$c_\alpha/c_\beta$
2HDM-Y-like	$\tan\beta$	$\cot\beta$	$-\cot\beta$	$c_\alpha/s_\beta$	$-s_\alpha/c_\beta$	$c_\alpha/s_\beta$	$s_\alpha/s_\beta$	$c_\alpha/c_\beta$	$s_\alpha/s_\beta$

TABLE II. Parameter expressions for the 2HDM-III like models, where  $s_\alpha \equiv \sin\alpha$ ,  $c_\alpha \equiv \cos\alpha$ ,  $s_\beta \equiv \sin\beta$  y  $c_\beta \equiv \cos\beta$ .

where

$$[\tilde{Y}_a^f]_{ij} = \frac{\sqrt{m_{f_i} m_{f_j}}}{v} [\tilde{\chi}_a^f]_{ij}. \quad (20)$$

The  $\tilde{\chi}_a^f$  matrices are responsible for inducing Flavor-Changing (FC) interactions at three-level. Finally using Eqs. (12)-(20) and by making use of the definitions in Ref. [32], we derive the Yukawa Lagrangian for quarks and the neutral scalar bosons  $\mathcal{L}_{ns}^Y$  given by

$$\begin{aligned} \mathcal{L}_{ns}^Y = & -\frac{g}{2M_W} \left[ \bar{d}_i \left( \left[ m_{d_i} \xi_H^d \delta_{ij} - \frac{(\xi_h^d + X \xi_H^d)}{f(X)} \frac{\sqrt{m_{d_i} m_{d_j}}}{\sqrt{2}} \tilde{\chi}_{ij}^d \right] H \right. \right. \\ & + \left. \left[ m_{d_i} \xi_h^d \delta_{ij} + \frac{(\xi_H^d - X \xi_h^d)}{f(X)} \frac{\sqrt{m_{d_i} m_{d_j}}}{\sqrt{2}} \tilde{\chi}_{ij}^d \right] h \right. \\ & + \left. i \left[ -m_{d_i} X \delta_{ij} + f(X) \frac{\sqrt{m_{d_i} m_{d_j}}}{\sqrt{2}} \tilde{\chi}_{ij}^d \right] \gamma^5 A \right) d_j \\ & + u_i \left( \left[ m_{u_i} \xi_H^u \delta_{ij} + \frac{(\xi_h^u - Y \xi_H^u)}{f(Y)} \frac{\sqrt{m_{u_i} m_{u_j}}}{\sqrt{2}} \tilde{\chi}_{ij}^u \right] H \right. \\ & + \left. \left[ m_{u_i} \xi_h^u \delta_{ij} - \frac{(\xi_H^u + Y \xi_h^u)}{f(Y)} \left( \frac{\sqrt{m_{u_i} m_{u_j}}}{\sqrt{2}} \right) \tilde{\chi}_{ij}^u \right] h \right. \\ & + \left. i \left[ -m_{u_i} Y \delta_{ij} + f(Y) \frac{\sqrt{m_{u_i} m_{u_j}}}{\sqrt{2}} \tilde{\chi}_{ij}^u \right] \gamma^5 A \right) u_j \Big], \end{aligned} \quad (21)$$

where  $f(x) = \sqrt{1+x^2}$  ( $x = X, Y, Z$ ). The remaining parameters are defined in the Table II. The Eq. (21) allows us to write a specific 2HDM plus FC interactions.

To compute the cross-section for  $pp \rightarrow th + X$ , we extract the coupling  $g_{tch}$  from Eq. (21)

$$g_{tch} = \frac{g}{2\sqrt{2}m_W} \frac{(\xi_H^u + Y \xi_h^u) \sqrt{m_t m_c}}{f(Y)} \tilde{\chi}_{tc}^u, \quad (22)$$

when the  $Y$ ,  $\xi_{H^0}^u$  and  $\xi_{h^0}^u$  parameters are replaced in Eq. (22), we can see that  $g_{tch}$  is the same for all the models of Table I, meaning that our results are valid for any of these models.

### C. Constraints on the 2HDM-III parameter space

We present a general overview of the 2HDM-III parameter space. Details of the analysis can be found in Ref. [33].

The model free parameters that have a direct impact on our predictions are:

1. Cosine of the difference of mixing angles:  $\cos(\alpha - \beta)$ ,
2. Ratio of the VEV's:  $\tan \beta$ ,
3. The parameter that changes flavor  $\chi_{tc}$  ( $\chi_{tc} \equiv \tilde{\chi}_{tc}^u$ ).

The observables we consider to be constraint are the following:

- LHC Higgs boson data [34, 35],
- Neutral meson physics  $B_s^0 \rightarrow \mu^+ \mu^-$  [36],  $B_d^0 \rightarrow \mu^+ \mu^-$  [36],
- $\ell_i \rightarrow \ell_j \ell_k \bar{\ell}_k$  and  $\ell_i \rightarrow \ell_j \gamma$  [37],
- Muon anomalous magnetic moment  $a_\mu$  [38].

The only parameter we did not consider in Ref. [33] is the matrix element  $\chi_{tc}$ , which is constrained by the upper limit on  $\mathcal{BR}(t \rightarrow ch)$  [19], as shown in Fig. 1.

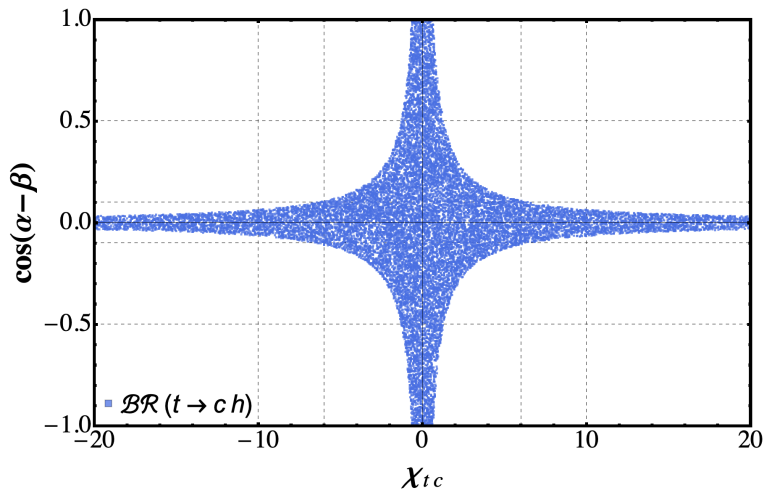


FIG. 1. Plot of  $\chi_{tc} - \cos(\alpha - \beta)$  plane. The colored points are allowed by the upper limit on  $\mathcal{BR}(t \rightarrow ch)$ .

We show in Fig. 2 the  $\cos(\alpha - \beta) - \tan \beta$  plane whose points correspond those allowed by 1) LHC Higgs boson data (green points), 2) Lepton Flavor Violating processes (yellow) and 3) upper limit on  $\mathcal{BR}(t \rightarrow ch)$  (blue points). We observe that the most stringent constraints come from the LHC Higgs boson data, which allow values for  $\cos(\alpha - \beta) \sim 0$  corresponding to the interval  $0.1 < \tan \beta < 50$ ; in agreement with the decoupling limit ( $\cos(\alpha - \beta) \rightarrow 0$ ).

The proposed process directly depends on the  $Y = \cot \beta$  factor, as shown in Eq. (22), it is clear that our signal is favored by small values of  $\tan \beta$ .

After a meticulous analysis of the model free parameters, we define three scenarios to be used in the next section:

- $S1$  :  $\tan \beta = 1$ ,  $\chi_{tc} = 1, 5, 10$  and  $\cos(\alpha - \beta) = 0.1$ ,
- $S2$  :  $\tan \beta = 3$ ,  $\chi_{tc} = 1, 5, 10$  and  $\cos(\alpha - \beta) = 0.1$ .

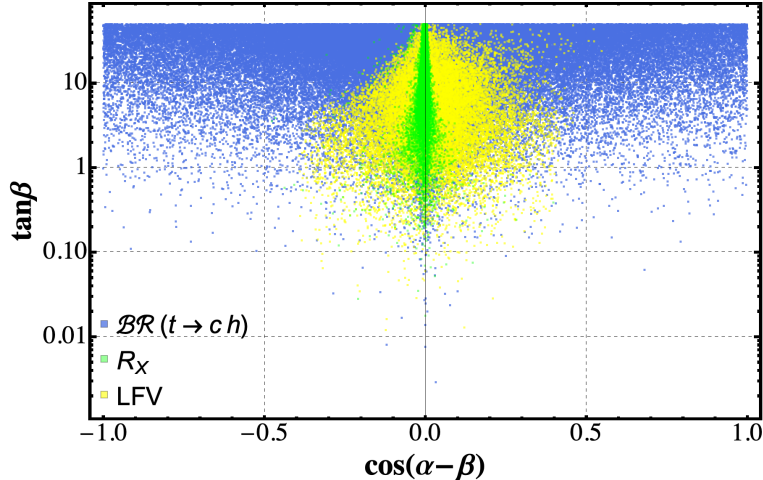


FIG. 2. Model parameter space of the 2HDM-III in the  $\cos(\alpha - \beta) - \tan\beta$  plane. The colored points are those allowed by LHC Higgs boson data (green), LFV processes (yellow) and upper limit on  $\mathcal{BR}(t \rightarrow ch)$ .

### III. COLLIDER ANALYSIS

In this section, we compute a Monte Carlo simulation and explore the prospects for detecting the proposed signal as well as the SM background processes that obscure it. In order to separate the signal from the background, we use the *Boosted Decision Trees* (BDT) machine learning algorithm [39] instead of making direct kinematic cuts as is commonly done.

#### A. Signal and background

We search for the process  $pp \rightarrow th + X$  ( $t \rightarrow \ell\nu_{\ell}b$ ,  $h \rightarrow \gamma\gamma$ ), whose Feynman diagrams that contribute to the signal are presented in Fig. 3. The red points indicate the new interaction coming from 2HDM-III, which induces the Flavor-Changing interaction. One of the most relevant observables of the signal is the resonant effect that comes from the decay  $h \rightarrow \gamma\gamma$ . Moreover, both photons show a transverse momentum such that their sum is approximately the mass of the Higgs boson, which is of utmost importance for the isolation of the signal. Meanwhile, the main SM background comes from  $Whj$ ,  $Wj\gamma\gamma$ ,  $tj\gamma\gamma$ ,  $Wjj\gamma$ ,  $tj\gamma$ , where  $j$  represents non-bottom-jets.

The cross-sections of the signal and the SM background processes are shown in Tables III and IV, respectively.

TABLE III. Cross-section of the signal for the scenarios  $S1$ ,  $S2$ .

Scenario	Cross-section [fb] ( $\chi_{tc} = 1$ )	Cross-section [fb] ( $\chi_{tc} = 5$ )
$S1$	0.01	0.025
$S2$	0.004	0.014

As far as our computation scheme is concerned, we first implement the full model via `FeynRules` [40] for



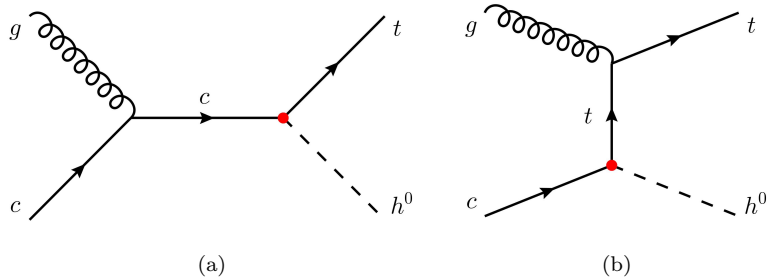


FIG. 3. Feynman diagrams for the process  $pp \rightarrow th$ , (a)  $s$ -channel and (b)  $t$ -channel.

TABLE IV. Cross-section of the dominant SM background processes.

SM backgrounds	Cross-section [fb]
$pp \rightarrow Whj$	0.19
$pp \rightarrow Wj\gamma\gamma$	68.27
$pp \rightarrow tj\gamma\gamma$	0.019
$pp \rightarrow Wjj\gamma$	16590
$pp \rightarrow tj\gamma$	1.84

the `MadGraph5` [41] event generator, interfaced with `Pythia8` [42] for parton showering, and finally we use `Delphes3` [43] for detector simulations. Concerning to the jet reconstruction, the finding package `FastJet` [44] and the `anti- $k_t$`  algorithm [45] package were used.

The traditional strategy of making hard cuts on the observables removes a significant number of background events but also refuses an important number of signal events. This situation can be improved by using MVA techniques, such as BDT. We perform a BDT training [39] using variables related to the kinematics of the final state, including the transverse momentum ( $p_T$ ) and the pseudo-rapidities of the  $b$ -jet, the charged lepton  $\ell$  and photons. We present in Fig. 4 the most discriminating training variables, plotted with `MadAnalysis5` [46]. The relevant hyperparameters for the BDT training are as follows: Number of trees `NTree=50`, maximum depth of the decision tree `MaxDepth=5`, maximum number of leaves `MaxLeaves=8`; the remaining parameters are set to their default values.

We present in Fig. 5 the discriminant for the signal and background. The goodness of fit is verified with the Kolmogorov-Smirnov (KS) test. We observed that the KS value lies within the allowed interval  $[0, 1]$  and has a value of 0.47 (0.59) for the signal (background). Once the classifier has been trained, it exports the output in terms of a single variable ( $\mathbf{xgb}$ ), which separates the signal events from the background, as shown in Fig. 5. Then, the signal-to-background ratio is optimized. The BDT training is computed using the Monte Carlo simulated data. The signal and background samples are scaled to the expected number of events, which is calculated via the integrated luminosity and cross-section values. The BDT selection is optimized individually for each channel to maximize the figure of merit, *i.e.*, the *signal significance*, defined as  $S/\sqrt{S+B}$ , where  $S$  and  $B$  represent the number of signal and background candidates respectively.

Fig. 6 presents our main results, *i.e.*, the *signal significance* as a function of the integrated luminosity for the two scenarios defined in the previous section:  $S1$ ,  $S2$ . We found that the scenario  $S1$  is the most promising, this because the cross-section for  $pp \rightarrow th + X$  is highly sensitive to low values of  $\tan \beta$  ( $g_{htc} \sim 1/\tan \beta$ ), as

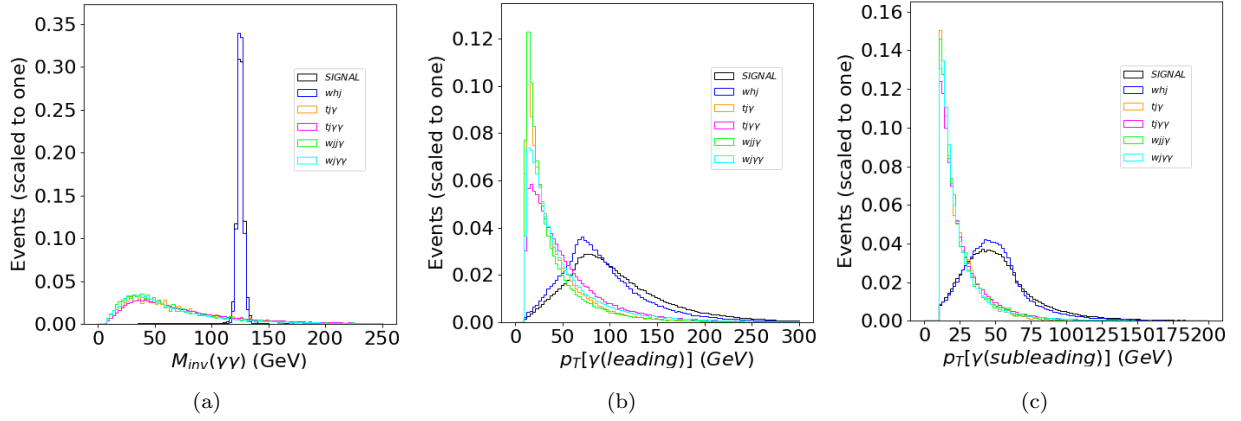


FIG. 4. Plots for the signal and background variables: (a) Invariant mass of the two photons, (b)  $p_T$  of the leading photon and (c)  $p_T$  of the subleading photon.

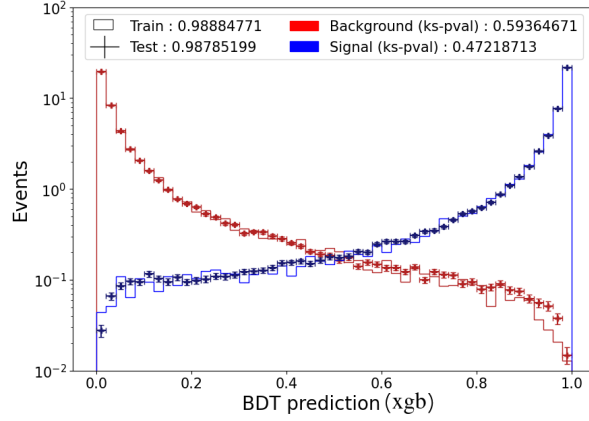


FIG. 5. Plot of the discriminant for signal and background data.

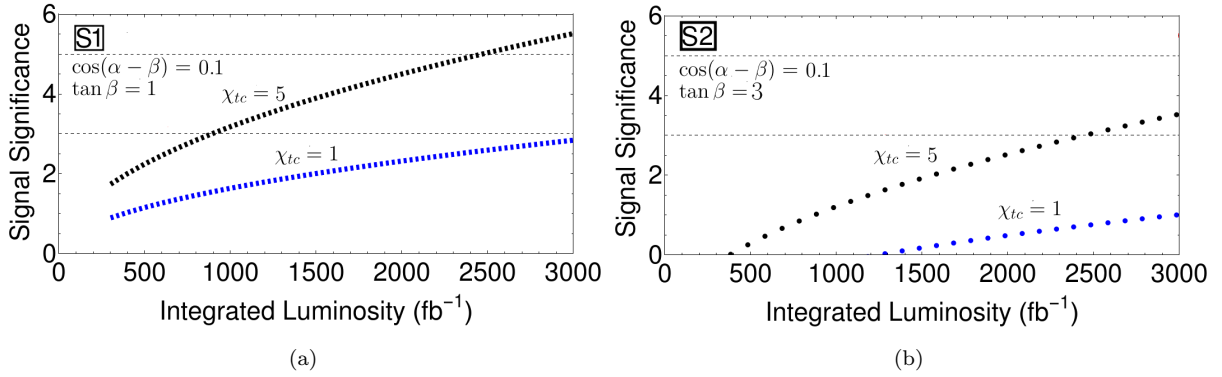


FIG. 6. *Signal significance* as a function of the integrated luminosity: (a) Scenario  $S1$ , (b) Scenario  $S2$

shown in Eq. (21). For scenario  $S1$  we predict a *signal significance*  $\sigma \geq 5$  ( $\sigma = 3$ ) for an integrated luminosity  $\mathcal{L}_{\text{int}} \geq 2500 \text{ fb}^{-1}$  ( $\mathcal{L}_{\text{int}} \sim 900 \text{ fb}^{-1}$ ) and  $\chi_{tc} = 5$ . This result indicates that in the HL-LHC experiment, evidence for the process  $pp \rightarrow th + X$  could be achieved. Meanwhile, scenario  $S2$  is the less favored because we set  $\tan\beta = 3$ ; although the *signal significance* for  $S2$  is relatively low, evidence for  $pp \rightarrow th + X$  can be achieved if a  $\mathcal{L}_{\text{int}} \sim 2500 \text{ fb}^{-1}$  is reached.

#### IV. CONCLUSIONS

The search for new physics is fundamental in collider experiments such as the LHC, particularly interesting are the Flavor-Violating processes which are very restricted in the SM. The 2HDM-III allows for this kind of interactions at tree-level that significantly increasing their production cross-sections. In this work, we have investigated the Flavor-Violating process  $pp \rightarrow th + X$ , which does not exist in the SM but has origin in the  $htc$  interaction predicted in the theoretical framework of the 2HDM-III.

We first have presented the relevant aspects of the 2HDM-III in which we studied prospects for detecting a single Higgs boson in association with a top quark. Specifically, we search for the final state  $t \rightarrow \ell\nu_{\ell}b$  and  $h \rightarrow \gamma\gamma$ , whose kinematic characteristics of the photons provided valuable information to isolate the signal from the background. The model parameter space was constrained on the basis of experimental results, namely, LHC Higgs boson data, upper limits on  $\mathcal{BR}(t \rightarrow ch)$  and relevant lepton FV processes. Using the previous results, we define two realistic scenarios  $S1$ ,  $S2$ . In order to increase the *signal significance*, we performed a Multivariate Analysis using BDT for the two scenarios. After using BDT, we found that the scenario  $S1$ :  $\tan\beta = 1$ ,  $\chi_{tc} = 1, 5$  and  $\cos(\alpha - \beta) = 0.1$ , is the most promising, which is expected since the  $htc \sim 1/\tan\beta$  interaction is favored for small values of  $\tan\beta$ . Our results allow us to predict a *signal significance* at level of  $\geq 5\sigma$  once the integrated luminosity  $\mathcal{L}_{\text{int}} \geq 2500 \text{ fb}^{-1}$  is reached. Given our results for the proposed signal, it is very likely that a future collider with higher center-of-mass energy may permit to achieve a higher significance for a broad range of parameters.

#### ACKNOWLEDGMENTS

The work of Marco A. Arroyo-Ureña and T. Valencia-Pérez is supported by “Estancias Posdoctorales por México (CONAHCYT)” and “Sistema Nacional de Investigadores” (SNI-CONAHCYT). T.V.P. acknowledges support from the UNAM project PAPIIT IN111224 and the CONAHCYT project CBF2023-2024-548. V.M.L.G. thanks to CONAHCYT México for the PhD fellowship. J.L.D.C. and O.F.B. thank the support of SNI-CONAHCYT.

- 
- [1] Georges Aad et al. Observation of a new particle in the search for the Standard Model Higgs boson with the ATLAS detector at the LHC. *Phys. Lett.*, B716:1–29, 2012.
  - [2] Serguei Chatrchyan et al. Observation of a new boson with mass near 125 GeV in pp collisions at  $\sqrt{s} = 7$  and 8 TeV. *JHEP*, 06:081, 2013.
  - [3] Peter Ware Higgs. Broken symmetries, massless particles and gauge fields. *Phys. Lett.*, 12:132–133, 1964.

- [4] Peter W. Higgs. Broken symmetries and the masses of gauge bosons. *Phys. Rev. Lett.*, 13:508–509, Oct 1964.
- [5] Peter W. Higgs. Spontaneous symmetry breakdown without massless bosons. *Phys. Rev.*, 145:1156–1163, May 1966.
- [6] F. Englert and R. Brout. Broken symmetry and the mass of gauge vector mesons. *Phys. Rev. Lett.*, 13:321–323, Aug 1964.
- [7] Various. Beyond the standard model of particle physics. *Philosophical Transactions of the Royal Society A*, 373(2047), 2015.
- [8] Hyun Min Lee. Lectures on physics beyond the standard model. *arXiv*, 1907.12409, 2019.
- [9] John Womersley. Beyond the standard model. *Symmetry Magazine*, n.d.
- [10] CERN. Beyond the standard model. <https://cds.cern.ch/record/2702850/files/937-4113-1-PB%20%282%29.pdf>, 2019.
- [11] Dris Boubaa, Gaber Faisel, and Shaaban Khalil. Beyond sm physics and searches for susy at the lhc. *arXiv*, 2005.08069, 2020.
- [12] Various. Anomalies in particle physics and their implications for new phenomena. *Nature Reviews Physics*, 2024.
- [13] D. Atwood, L. Reina, and A. Soni. Flavor changing neutral currents in the two higgs doublet model type iii. *Physical Review D*, 55:3156–3176, 1997.
- [14] A. Arhrib, R. Benbrik, M. Chabab, G. Moultaqa, et al. Higgs phenomenology in the two higgs doublet model type iii. *Physical Review D*, 84:095005, 2011.
- [15] O. Félix-Beltrán, F. González-Canales, J. Hernández-Sánchez, S. Moretti, R. Noriega-Papaqui, and A. Rosado. Analysis of the quark sector in the 2HDM with a four-zero Yukawa texture using the most recent data on the CKM matrix. *Phys. Lett. B*, 742:347–352, 2015.
- [16] Nivedita Ghosh and Jayita Lahiri. Generalized 2HDM with wrong-sign lepton-Yukawa coupling, in light of  $g_\mu - 2$  and lepton flavor violation at the future LHC. *Eur. Phys. J. C*, 81(12):1074, 2021.
- [17] Marco A. Arroyo-Ureña, J. Lorenzo Díaz-Cruz, Enrique Díaz, and Javier A. Orduz-Ducuara. Flavor violating Higgs signals in the Texturized Two-Higgs Doublet Model (THDM-Tx). *Chin. Phys. C*, 40(12):123103, 2016.
- [18] S. L. Glashow, J. Iliopoulos, and L. Maiani. Weak Interactions with Lepton-Hadron Symmetry. *Phys. Rev. D*, 2:1285–1292, 1970.
- [19] Georges Aad et al. Search for flavour-changing neutral current interactions of the top quark and the Higgs boson in events with a pair of  $\tau$ -leptons in pp collisions at  $\sqrt{s} = 13$  TeV with the ATLAS detector. *JHEP*, 2306:155, 2023.
- [20] Aram Hayrapetyan et al. Search for flavor-changing neutral current interactions of the top quark mediated by a Higgs boson in proton-proton collisions at 13 TeV. 7 2024.
- [21] Nuno Filipe Castro and Kirill Skovpen. Flavour-Changing Neutral Scalar Interactions of the Top Quark. *Universe*, 8(11):609, 2022.
- [22] Yao-Bei Liu and Zhen-Jun Xiao. Searches for the FCNC couplings from top-Higgs associated production signal with  $h \rightarrow \gamma\gamma$  at the LHC. *Phys. Lett. B*, 763:458–464, 2016.
- [23] G. Apollinari, O. Brüning, T. Nakamoto, and Lucio Rossi. High Luminosity Large Hadron Collider HL-LHC. *CERN Yellow Rep.*, (5):1–19, 2015.
- [24] G. C. Branco, P. M. Ferreira, L. Lavoura, M. N. Rebelo, Marc Sher, and Joao P. Silva. Theory and phenomenology of two-Higgs-doublet models. *Phys. Rept.*, 516:1–102, 2012.
- [25] J. Lorenzo Díaz-Cruz. The Higgs profile in the standard model and beyond. *Rev. Mex. Fis.*, 65(5):419–439, 2019.
- [26] P. A. Zyla et al. Review of Particle Physics. *PTEP*, 2020(8):083C01, 2020.
- [27] M. Ashry, S. Khalil, and S. Moretti. Searching for a heavy neutral CP-even Higgs boson in the BLSSM at the LHC Run 3 and HL-LHC. *Eur. Phys. J. C*, 84(4):433, 2024.
- [28] S. Kuday, H. Saygin, İ. Hoş, and F. Çetin. Projections for Neutral Di-Boson and Di-Higgs Interactions at FCC-he Collider. *Nucl. Phys. B*, 932:1–14, 2018.
- [29] Siba Prasad Das, Marek Nowakowski, J. Hernández-Sánchez, Stefano Moretti, and Alfonso Rosado. Neutral and Charged Higgs boson phenomenology at the LHeC and FCC-eh. In

38th International Symposium on Physics in Collision, 12 2018.

- [30] J. L. Díaz-Cruz, R. Noriega-Papaqui, and A. Rosado. Mass matrix ansatz and lepton flavor violation in the two-higgs doublet model-iii. *Phys. Rev. D*, 69:095002, May 2004.
- [31] J. L. Díaz-Cruz, R. Noriega-Papaqui, and A. Rosado. Measuring the fermionic couplings of the higgs boson at future colliders as a probe of a nonminimal flavor structure. *Physical Review D*, 71(1), January 2005.
- [32] J. Hernandez-Sanchez, S. Moretti, R. Noriega-Papaqui, and A. Rosado. Off-diagonal terms in Yukawa textures of the Type-III 2-Higgs doublet model and light charged Higgs boson phenomenology. *JHEP*, 07:044, 2013.
- [33] M. A. Arroyo-Ureña, E. A. Herrera-Chacón, S. Rosado-Navarro, and Humberto Salazar. Hunting a charged Higgs boson pair in proton-proton collisions. 5 2024.
- [34] Albert M Sirunyan et al. Search for lepton flavour violating decays of the Higgs boson to  $\mu\tau$  and  $e\tau$  in proton-proton collisions at  $\sqrt{s} = 13$  TeV. *JHEP*, 06:001, 2018.
- [35] Georges Aad et al. Searches for lepton-flavour-violating decays of the Higgs boson in  $\sqrt{s} = 13$  TeV pp collisions with the ATLAS detector. *Phys. Lett. B*, 800:135069, 2020.
- [36] Armen Tumasyan et al. Measurement of the  $B_S^0 \rightarrow \mu^+ \mu^-$  decay properties and search for the  $B^0 \rightarrow \mu^+ \mu^-$  decay in proton-proton collisions at  $\sqrt{s} = 13$  TeV. *Phys. Lett. B*, 842:137955, 2023.
- [37] R. L. Workman and others (Particle Data Group). Review of Particle Physics. *Prog. Theor. Exp. Phys.*, 2022:083C01, 2022.
- [38] B. Abi et al. Measurement of the Positive Muon Anomalous Magnetic Moment to 0.46 ppm. *Phys. Rev. Lett.*, 126(14):141801, 2021.
- [39] Katherine Woodruff and on behalf of the MicroBooNE collaboration. Automated proton track identification in microboone using gradient boosted decision trees. *Journal of Physics: Conference Series*, 1085(4):042019, sep 2018.
- [40] Adam Alloul, Neil D. Christensen, Céline Degrande, Claude Duhr, and Benjamin Fuks. FeynRules 2.0 - A complete toolbox for tree-level phenomenology. *Comput. Phys. Commun.*, 185:2250–2300, 2014.
- [41] J. Alwall, R. Frederix, S. Frixione, V. Hirschi, F. Maltoni, O. Mattelaer, H. S. Shao, T. Stelzer, P. Torrielli, and M. Zaro. The automated computation of tree-level and next-to-leading order differential cross sections, and their matching to parton shower simulations. *JHEP*, 07:079, 2014.
- [42] Torbjörn Sjöstrand, Stefan Ask, Jesper R. Christiansen, Richard Corke, Nishita Desai, Philip Ilten, Stephen Mrenna, Stefan Prestel, Christine O. Rasmussen, and Peter Z. Skands. An introduction to PYTHIA 8.2. *Comput. Phys. Commun.*, 191:159–177, 2015.
- [43] J. de Favereau, C. Delaere, P. Demin, A. Giammanco, V. Lemaître, A. Mertens, and M. Selvaggi. DELPHES 3, A modular framework for fast simulation of a generic collider experiment. *JHEP*, 02:057, 2014.
- [44] Matteo Cacciari, Gavin P. Salam, and Gregory Soyez. FastJet User Manual. *Eur. Phys. J. C*, 72:1896, 2012.
- [45] Matteo Cacciari, Gavin P. Salam, and Gregory Soyez. The anti- $k_t$  jet clustering algorithm. *JHEP*, 04:063, 2008.
- [46] Eric Conte, Benjamin Fuks, and Guillaume Serret. MadAnalysis 5, A User-Friendly Framework for Collider Phenomenology. *Comput. Phys. Commun.*, 184:222–256, 2013.